ELSEVIER

Journal of Chromatography A, 955 (2002) 95–103

JOURNAL OF CHROMATOGRAPHY A

www.elsevier.com/locate/chroma

# Different elution modes and field programming in gravitational field-flow fractionation
# IV. Field programming achieved with channels of non-constant cross-sections

Jana Plocková*, František Matulík, Josef Chmelík

*Institute of Analytical Chemistry, AS CR, 611 42 Brno, Czech Republic*

Received 18 September 2001; received in revised form 5 February 2002; accepted 20 February 2002

**Abstract**

Force field programming provided increased speed of separation with an improved resolution and detection capability in many field-flow fractionation (FFF) techniques. Gravitational field-flow fractionation (GFFF) uses the Earth's gravitational field to cause the settlement of particles towards the channel accumulation wall. Although this field is constant and relatively weak, there are different ways to implement force field programming in GFFF. Because hydrodynamic lift forces (HLF) participate in the separation process in focusing (hyperlayer) elution mode, they can control the resulting force field acting on particles via changes in flow-velocity. These changes can be accomplished by a programmable pump or with channels of non-constant cross-sections. This work is focused on flow-velocity programming accomplished with channels of non-constant cross-sections. Three trapezoidal channels of decreasing breadth and two channels of decreasing height (along the longitudinal axis) are tested as tools for optimization of the separation of a model silica gel particle mixture. The trapezoidal channels yielded reduced separation times. However, taking into account both speed of separation and resolution, the optimization effect was lower compared with the flow-rate gradients generated by a programmable pump. The channels of non-constant height did not yield advantageous separations. 

*Keywords:* Gravitational field-flow fractionation; Field programming; Hydrodynamic lift forces; Flow-velocity gradients; Field-flow fractionation

## 1. Introduction

Field-flow fractionation (FFF) is an analytical method based on the simultaneous actions of a non-uniform flow velocity profile of a carrier liquid and an applied transverse force field [1]. Gravitational field-flow fractionation (GFFF) uses the Earth's gravitational field as the external force field that causes settlement of particles towards the channel accumulation wall. However, some other forces participate in the separation process when μm-sized sample particles elute in the carrier liquid flow. The most important of them are the hydrodynamic lift forces (HLF) [2]. They tend to drive the particles away from the channel accumulation wall (i.e. against the sedimentation force) and to focus them into narrow zones. These zones are then located in

*Corresponding author.

*E-mail address:* plockova@iach.cz (J. Plocková).

0021-9673/02/$ – see front matter 
PII: S0021-9673(02)00195-4

the flow velocity profile at those positions where the effective particle weight equals HLF. It follows that any change in these counteracting forces results in a change in retention ratio. The elution mode is called focusing (hyperlayer) [3,4].

Because no technical device generating the external force field is required, the experimental GFFF arrangement is the simplest and cheapest among the family of FFF techniques [5]. GFFF has been successfully applied to separation, characterisation and micropreparation of a wide variety of particulate materials [6–17]. The advantage of the technical simplicity and low cost of GFFF apparatus as well as the gentle separation conditions desirable for the treatment of living cells evoke further efforts to broaden the applicability and separation capabilities of this technique.

Force field programming provided increased speed of analysis with an improved resolution and detection capability in many FFF techniques [18–21]. Although the Earth's gravitational field is constant and relatively weak, there are different ways to implement force field programming in GFFF. In Ref. [22], the theoretical analysis of the mechanisms of different elution modes in GFFF was used to suggest several possibilities, how to control the resulting force field acting on particles: the resulting force acting on particles can be modulated by changing the angle between the Earth's gravitational field and the longitudinal axis of the channel and by the use of carrier liquids having different densities. Furthermore, in focusing elution mode, the resulting force acting on particles is a function of two counteracting forces (the Earth's gravity and HLF). Thus, HLF can be employed for programming of the resulting force field [22].

Several mathematical formulae have been suggested to describe HLF action [23,24]. The magnitude of the inertial lift force (when the particle is relatively far away from the channel wall) can be calculated according to Eq. (1) [25]:

$$F_I = -\frac{81}{4}\pi\rho_{cl}u^2\frac{r^4}{w^2}(1-2\delta)\frac{K^2-(1-2\delta)^2}{1-K^2} \qquad (1)$$

where $F_I$ is the inertial lift force, $\rho_{cl}$ is the density of the carrier liquid, $u$ is the average linear velocity of the carrier liquid, $r$ is the particle radius, $w$ is the channel height, $\delta$ is the dimensionless distance of the particle center from the channel bottom ($\delta = x/w$, where $x$ is the absolute distance and $w$ is the channel height) and $K = 0.62$. This equation does not describe thoroughly the behaviour of particles in the close vicinity to the channel wall. For the near-wall lift force (i.e. the force of non-inertial origin acting additionally on particles in the region very near to the wall), an empirical relation was obtained [23]:

$$F_{NW} = 6C\eta u\frac{r^3}{hw} \qquad (2)$$

where $F_{NW}$ is the near-wall lift force, $C$ is an empirical constant, $\eta$ is the dynamic viscosity of the carrier liquid, and $h$ is the closest distance between the particle surface and the channel bottom.

It is shown that the magnitude of HLF increases with increasing flow-velocity, with decreasing channel height, with increasing particle radius, with increasing viscosity of the carrier liquid and depends dramatically on the position in the channel height cross-section. It follows that we can modulate the HLF action and thus the resulting force field acting on given particles by changing the flow-velocity or/and varying the channel height. There are two possibilities to achieve the flow-velocity changes [22]: beside straightforward flow-rate programming by programmable pump the utilization of channels with non-constant cross-sections is the other way, which is described in this paper. Whereas channels of non-constant breadth provide simple flow-velocity gradients, in the channel of non-constant height (along the longitudinal axis), the effect of the flow-velocity gradient resulting from the non-constant cross-section is combined with the effect of decreasing channel height (see Eq. (1)).

The phenomena considered in Ref. [22] were experimentally demonstrated using silica spheres as model particles in Ref. [26], where a properly functioning range of experimental conditions for the suggested flow-rate and carrier liquid density gradients was described. Refs. [27,28] deal with force field programming accomplished by a programmable pump. Several flow-rate gradients (step gradients, linear gradients, parabolic, and combined ones) were tested as tools for optimization of the separation of starch granules and silica gel particle mixture. Some

flow-rate gradients presented in Ref. [28] provided better resolution of the first two peaks (these silica samples have overlapping particle size distributions, see the fractograms in Fig. 2) and baseline resolution of the last two peaks (their particle size distributions do not overlap) at shorter separation time.

This work is focused on flow-velocity programming accomplished with channels of non-constant cross-sections. The channels of different geometry (three trapezoidal channels of decreasing breadth and two channels of decreasing height along the longitudinal axis) are implemented in force field programming in GFFF. Trapezoidal cross-section channels have been previously employed in FFF for gradient techniques, where asymmetric flow velocity profiles were used [29,30]. These velocity profiles were then described mathematically [31,32]. A trapezoidal channel of decreasing breadth was introduced for the first time in flow FFF [33]. The trapezoidal geometry was implemented in order to minimize changes in the flow velocity of carrier liquid along the asymmetrical flow FFF channel [34]. The channel of decreasing height (along the longitudinal axis) was devised and constructed in our laboratory. The intended effect was to amplify the influence of increasing flow-velocity resulting from the decreasing cross-section by the effect of decreasing channel height.

The aim of this work is to describe the influence of flow-velocity gradients generated by channels of decreasing height and channels of decreasing breadth on the separation using the same model mixture as that in Ref. [28]. The optimizing effect, experimental advantages and drawbacks are compared with those achieved by a programmable pump.

## 2. Experimental

Seven different channels, two rectangular, three trapezoidal and two channels of non-constant height have been assembled. The dimensions of the channels are reported in Table 1. The length of all the channels (the distance between the inlet and outlet capillaries) was 35 cm from tip to tip except channel B, which was 30 cm. The length of the tapered ends was 3 cm except the outlets of the trapezoidal channels, which were shorter (Fig. 1). The rectangular channels and the trapezoidal ones were cut in a spacer and assembled in the same manner as described in previous studies [7]. The construction of the channels of decreasing height was as follows: the inlet-tapered end was cut from the spacer of thickness $w_1$ (Table 1) and the outlet-tapered end from the spacer of thickness $w_2$. These inlet and outlet pieces of spacer were properly sandwiched (defining the length of the channel) between two float glass plates of 2-cm breadth in order to support the

Table 1
Dimensions of the channels

| Channel | $w$ (μm) | $w_1$ (μm) | $w_2$ (μm) | $B_1$ (mm) | $B_2$ (mm) | $D$ (mm) | $V_0$ (ml) |
|---|---|---|---|---|---|---|---|
| *Rectangular channels* | | | | | | | |
| A | 80 | – | – | 20 | 20 | 290 | 0.49 |
| B | 150 | – | – | 20 | 20 | 240 | 0.82 |
| *Channels of non-constant breadth* | | | | | | | |
| C | 80 | – | – | 20 | 10 | 305 | 0.37 |
| D | 80 | – | – | 20 | 5 | 312.5 | 0.31 |
| E | 80 | – | – | 20 | 1.5 | 317.8 | 0.27 |
| *Channels of non-constant height* | | | | | | | |
| F | – | 80 | 40 | 20 | 20 | 290 | 0.36 |
| G | – | 150 | 80 | 20 | 20 | 290 | 0.69 |

$B_1$, the base of the inlet triangle (Fig. 1); $B_2$, the base of the outlet triangle (Fig. 1); $D$, the distance between the bases of the inlet and outlet triangles; $w$, the constant channel height of the rectangular and trapezoidal channels; $w_1$, the height of the inlet apex (Fig. 1); $w_2$, the height of the outlet apex (Fig. 1); $V_0$, geometrical void volume. Because of the stop-flow injection procedure [7], $V_0$ does not include the inlet apex.

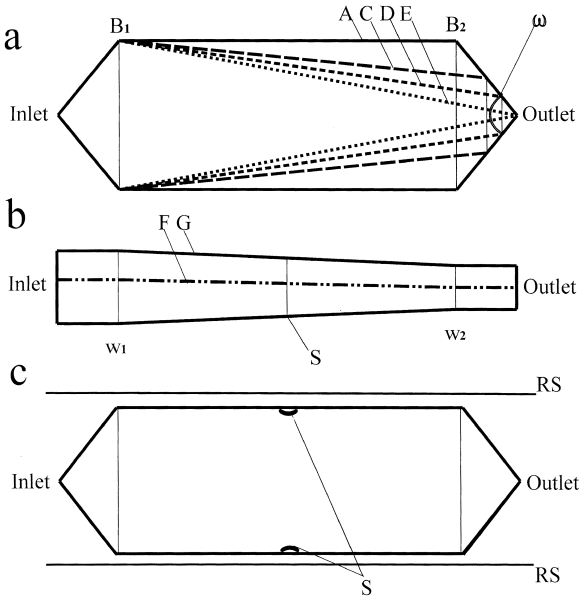


Fig. 1. (a) Schematic illustration of the rectangular channel A and the trapezoidal channels C, D and E. $B_1$ is the base of the inlet triangle, $B_2$ denotes the bases of the outlet triangles. The angle $\omega$ of the outlet remains the same for all the channels except channel E, where the channel breadth gradient converges straight to the outlet capillary without any outlet triangle. The stronger the channel breadth gradient (channels C, D), the shorter is $B_2$ and also the altitude of the outlet triangle. As the altitude of the outlet triangle decreases, the distance between $B_1$ and $B_2$ increases. (b) Cross-section of channels F and G with non-constant height. The symbols $w_1$ and $w_2$ designate the heights of the inlet and outlet apices, respectively. The channel dimensions are specified in Table 1. The symbol S denotes the half-length, where the tiny supports of proper height are located at the edges of the channel. (c) Schema (the view from above) of channels F and G with non-constant height. The symbol S denotes the tiny supports of proper height. The rubber belts used as a gasket sealing the lateral walls are labelled RS.

channel at two height extremes. In order to ensure a linear height gradient, two more tiny supports of proper height (i.e. 60 μm for channel F and 115 μm for channel G) were inserted in the half-length of the channel in this manner: one piece from the left side of the channel and one piece from the right side (Fig. 1c). The pieces were anchored at the edges of the glass plate in order not to be wafted by the stream. Two rubber belts were applied as side walls of the channel. They were gripped to glass plates with metal construction. The glass plates were then clamped together with two Plexiglas bars.

The system operated with a HP 1100 Series Quaternary Pump (Hewlett-Packard) and a UVM 4 spectrophotometric detector (Development Workshops AS CR, Prague, Czech Republic). The detector was equipped with a Z-shaped cell with an optical path of 5 mm and was set on 254 nm. Milli-Q water was used as the carrier liquid.

The model mixture consisted of non-porous silica gel particles of diameter 1.6 μm (a gift from Professor E. Kováts, SFIT, Lausanne, Switzerland) and porous ones (Sepharon SGX) of nominal diameters 5 and 10 μm (Tessek, Prague, Czech Republic). The mixture preparation has been described in detail in Ref. [28]. The concentrations of particular analytes in the model mixture were as follows: 2.7 mg/ml of the analyte 1 (10 μm), 2.7 mg/ml of the analyte 2 (5 μm) and 0.7 mg/ml of the analyte 3 (1.6 μm). A 2-μl volume of the model mixture was injected. The stop-flow time [8] was 60 s.

## 3. Results and discussion

As described in the previous work [28], the model mixture contains two analytes with a broad overlapping size distribution ($d=5$ μm, polydispersity $P=1.12$, $d=10$ μm, $P=1.14$). This results in wide and significantly overlapping peaks 1 and 2 [7]. Moreover, the peaks are not Gaussian, which rules out the convention for calculation of peak resolution when the peaks are not baseline separated. Our non-standard situation requires an appropriate parameter for evaluation of peak resolution obtained under the conditions of the tested gradients. In the previous work [28], we arbitrarily defined parameters $R^*_{1,2}$ and $R^*_{2,3}$ by Eqs. (3) and (4) as follows:

$$R^*_{1,2} = \frac{b-a}{\alpha+\beta} \quad (3)$$

$$R^*_{2,3} = \frac{c-b}{\gamma+\delta} \quad (4)$$

where $a$ is the elution time of peak 1, $b$ is the elution time of peak 2 and $c$ is the elution time of peak 3. $\alpha$, $\beta$, $\gamma$ and $\delta$ are adjoining half-widths of the peaks taken at one-half of their heights. $\alpha$ is the tailing half-width of the peak 1, $\beta$ is the fronting half-width of peak 2, $\gamma$ is the tailing half-width of peak 2 and $\delta$

is the fronting half-width of peak 3. It is reasonable to use the same parameters for the evaluation of the gradient separations in this work. We evaluated only the separations yielding $R^*_{1,2}>1$. The separations yielding $R^*_{1,2}<1$ are considered to be unsuccessful. In order to involve separation time in the evaluation, we arbitrarily defined parameters $P_{1,2}$ and $P_{2,3}$ by Eqs. (5) and (6) for the final comparison of the successful separations:

$$P_{1,2} = \frac{R^*_{1,2}}{b} \quad (5)$$

$$P_{2,3} = \frac{R^*_{2,3}}{c} \quad (6)$$

Fig. 2 presents fractograms of the model mixture obtained in the rectangular channel A ($w=80$ μm) at three constant flow-rates (Fig. 2a–c) and in the rectangular channel B ($w=150$ μm) at the flow-rate 1 ml/min (Fig. 2d). In channel A, the increasing retention ratios with increasing flow-rate confirm the mechanism of focusing elution mode induced by HLF. The best resolution was obtained at the flow-rate 0.2 ml/min ($R^*_{1,2}=1.4$, $R^*_{2,3}=4.3$), however, the total separation time was 19 min. At the flow-rates 0.5 and 1 ml/min, the speed of separation increased at the expense of resolution, which is documented by the drop in the parameter $R^*_{1,2}$ below the value of 1. The total separation times were 6.4 and 3 min. In channel B, the lower retention ratios compared with channel A at the same linear flow-rate correspond to the increased channel height. Total separation time was 7.7 min and the values of $R^*$ were as follows: $R^*_{1,2}=1.2$, $R^*_{2,3}=4.6$.

Fractionations accomplished under the conditions of the moderate flow-velocity gradient generated by the trapezoidal channel C are reported in Fig. 3. The time reduction (compared with Fig. 2) was not associated with degradation of peak resolution at any flow-rate. At the flow-rate of 0.5 ml/min, the resolution of the first two peaks was even improved. The achieved total separation times and values of $R^*$ were as follows: 15 min, $R^*_{1,2}=1.4$, $R^*_{2,3}=3.3$ at the flow-rate 0.2 ml/min; 5.2 min, $R^*_{1,2}=1.1$, $R^*_{2,3}=3.3$ at the flow-rate 0.5 ml/min and 2.4 min, unsuccessful separation at the flow-rate 1 ml/min.

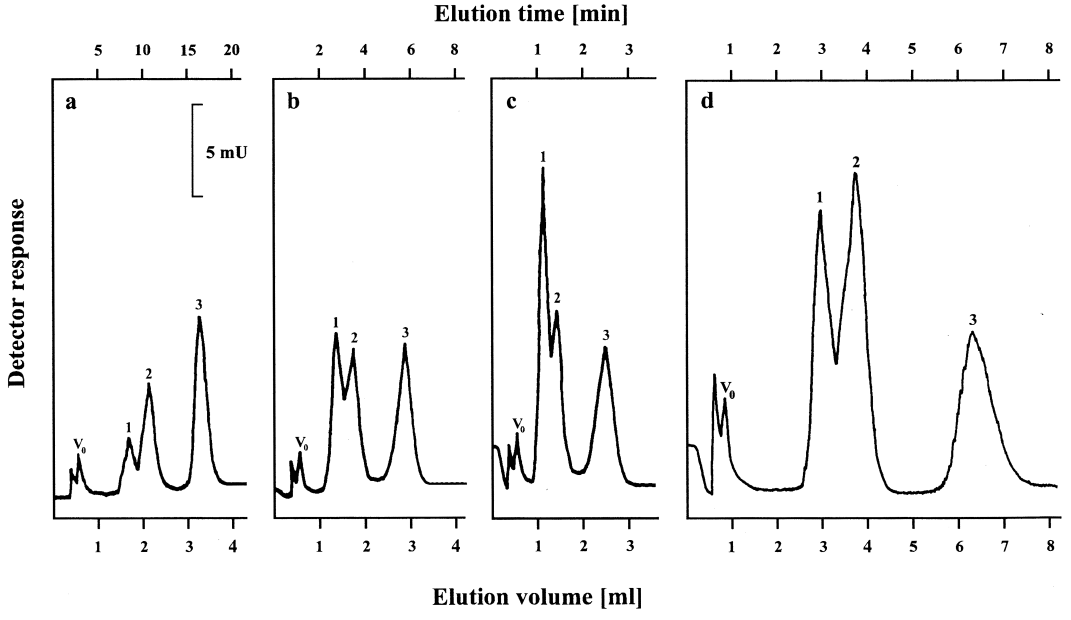


Fig. 2. Fractograms of the model silica mixture obtained in the rectangular channel A at the flow-rates: (a) 0.2 ml/min, (b) 0.5 ml/min and (c) 1.0 ml/min and in the rectangular channel B at the flow-rate 1.0 ml/min (d). The peak corresponding to void volume is designated by $V_0$ and the peaks 1, 2, and 3 refer to the analytes 1 (10 μm), 2 (5 μm), and 3 (1.6 μm), respectively. The separations have been evaluated as follows: (a) $R^*_{1,2}=1.4$, $R^*_{2,3}=4.3$, (b) unsuccessful, (c) unsuccessful, (d) $R^*_{1,2}=1.2$, $R^*_{2,3}=4.6$.

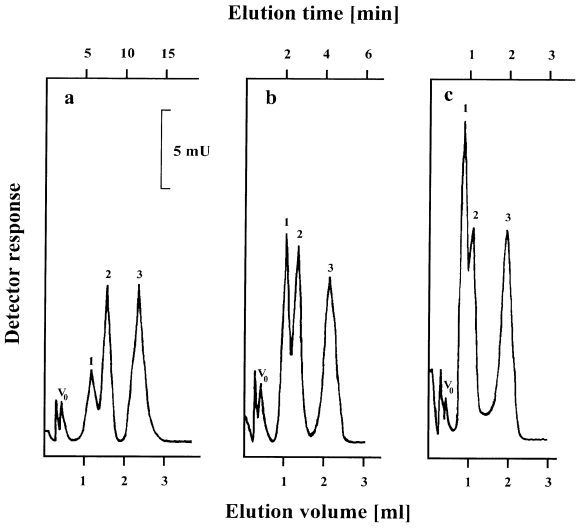


Fig. 3. Fractograms of the model silica mixture obtained in the trapezoidal channel C at the flow-rates: (a) 0.2 ml/min, (b) 0.5 ml/min and (c) 1.0 ml/min. The symbols $V_0$, 1, 2, and 3 are used in the same way as in Fig. 2. The evaluation: (a) $R^*_{1,2}=1.4$, $R^*_{2,3}=3.3$, (b) $R^*_{1,2}=1.1$, $R^*_{2,3}=3.3$, (c) unsuccessful.

The enhanced flow-velocity gradient generated by the trapezoidal channel D (Fig. 4) provided additional time reduction, while the value of $R^*_{1,2}$ at the flow-rate 0.2 ml/min remained the same ($R^*_{1,2}=1.4$, $R^*_{2,3}=2.9$). However, at the flow-rate 0.5 ml/min, the resolution of the first two peaks was affected (unsuccessful separation). The total separation times were 12.2 min at the flow-rate 0.2 ml/min, 4.7 min at the flow-rate 0.5 ml/min and 2.2 min at the flow-rate 1 ml/min.

The separations obtained in the trapezoidal channel E are presented in Fig. 5. As the flow-velocity gradient provided by the channel geometry intensifies (the velocity at the outlet increased 3.3 times compared with channel D), the height of peak 1 increases (due to the enhanced focusing and elevating effect of HLF) and the resolution of the first two peaks degrades till no resolution is observed (Fig. 5c). Based on the parameter $R^*_{1,2}$ the separations in Fig. 5 are unsuccessful. The total separation times are 11.3 min at the flow-rate 0.2 ml/min, 4.5 min at the flow-rate 0.5 ml/min and 2.0 min at the flow-rate 1 ml/min.

In Table 2, the separations obtained in channels A, C and D are evaluated by the values of the parameters $R^*_{1,2}$, $R^*_{2,3}$ and $P_{1,2}$, $P_{2,3}$. Table 2 does not include channel E, because no successful separation

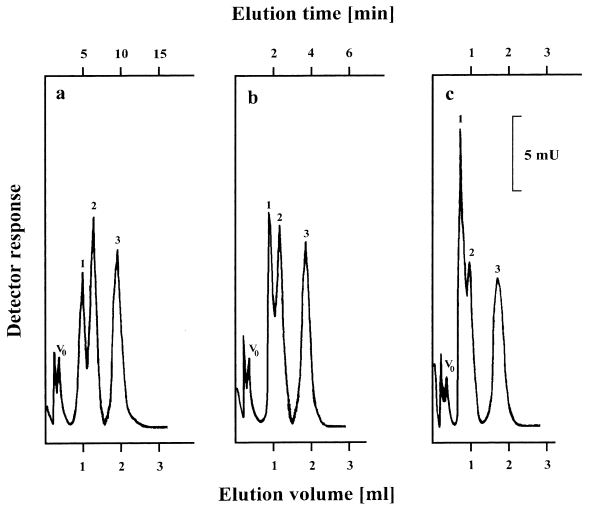


Fig. 4. Fractograms of the model silica mixture obtained in the trapezoidal channel D at the flow-rates: (a) 0.2 ml/min, (b) 0.5 ml/min and (c) 1.0 ml/min. The symbols $V_0$, 1, 2, and 3 are used in the same way as in Fig. 2. The evaluation: (a) $R^*_{1,2}=1.4$, $R^*_{2,3}=2.9$, (b) unsuccessful, (c) unsuccessful.

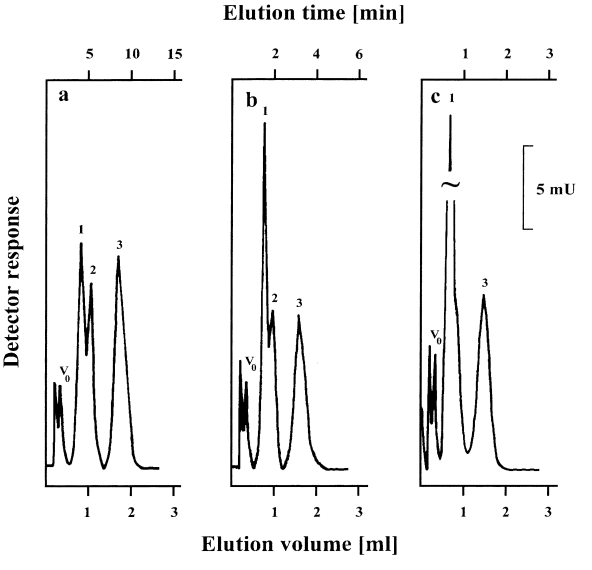


Fig. 5. Fractograms of the model silica mixture obtained in the trapezoidal channel E at the flow-rates: (a) 0.2 ml/min, (b) 0.5 ml/min and (c) 1.0 ml/min. The symbols $V_0$, 1, 2, and 3 are used in the same way as in Fig. 2. The evaluation: (a) unsuccessful, (b) unsuccessful, (c) unsuccessful.

Table 2
The evaluation of the trapezoidal channels based on the achieved values of the parameters $R^*_{1,2}$, $R^*_{2,3}$ and $P_{1,2}$, $P_{2,3}$

| Channel | Flow-rate | | | | |
|---|---|---|---|---|---|
| | 0.2 ml/min | | 0.5 ml/min | | 1.0 ml/min |
| A | $R^*_{1,2}=1.4$ | $P_{1,2}=0.13$ | Unsuccessful | | Unsuccessful |
| | $R^*_{2,3}=4.3$ | $P_{2,3}=0.26$ | separation | | separation |
| C | $R^*_{1,2}=1.4$ | $P_{1,2}=0.18$ | $R^*_{1,2}=1.1$ | $P_{1,2}=0.41$ | Unsuccessful |
| | $R^*_{2,3}=3.3$ | $P_{2,3}=0.28$ | $R^*_{2,3}=3.3$ | $P_{2,3}=0.79$ | separation |
| D | $R^*_{1,2}=1.4$ | $P_{1,2}=0.22$ | Unsuccessful | | Unsuccessful |
| | $R^*_{2,3}=2.9$ | $P_{2,3}=0.30$ | separation | | separation |

was achieved with it. It is obvious that taking into account the impact of both the resolution and separation time (provided that the requirement $R^*_{1,2}>1$ is fulfilled), the best result was achieved with the trapezoidal channel C at the flow-rate 0.5 ml/min ($P_{1,2}=0.41$). At the flow-rate 0.2 ml/min, channel D yielded better separation ($P_{1,2}=0.22$) than channel C ($P_{1,2}=0.18$).

If we program a force field, we change not only separation time but also retention ratio. The comparison of Figs. 2–5 shows that as the flow-velocity gradient stepwise enhances (channel A→C→D→E), the retention ratios slightly increase. This phenomenon is obvious at each particular flow-rate (compare Figs. 2a–5a, Figs. 2b–5b, and Figs. 2c–5c). It confirms that modulation of the resulting force field occurs.

The invention of the channel with non-constant height was not easy to assembly. In spite of the attention paid to a gasket sealing the lateral walls of these channels, we did not manage to prevent leakage of carrier liquid at higher flow-rates. Therefore, the highest applicable flow-rate for channel F was 0.4 ml/min and for channel G, 0.8 ml/min. The fractograms of the model mixture obtained in channels F and G at the highest applicable flow-rates are reported in Fig. 6. These fractograms obviously differ from those reported in Figs. 2–5. First, in both Fig. 6a and 6b, the ratio of peak heights of the first two peaks is inverse to that expected. Second, the last peak emerging from channel F is significantly broadened compared to Fig. 3. It should be emphasised that the flow-velocity gradient generated by channel F is comparable to that generated by channel C, because the outlet cross-sections of both the channels are half of their inlet cross-sections. In channel F, the additional effect of decreasing channel height was expected to amplify the potential of flow-velocity gradient. This superposed effect should cause higher retention ratios than obtained in channel C. The retention ratios observed in channel F at the flow-rate 0.4 ml/min are slightly lower than those obtained in channel C at the flow-rate 0.2 ml/min. Total separation time achieved in channel F is 8.7 min. According to the parameter $R^*_{1,2}=2.7$, the separation in channel F (Fig. 6a) would seem to be very successful, however, the broadening of peak 3 did not support this consideration.

The retention ratios obtained in channel F are expectedly higher than those ones obtained in chan-

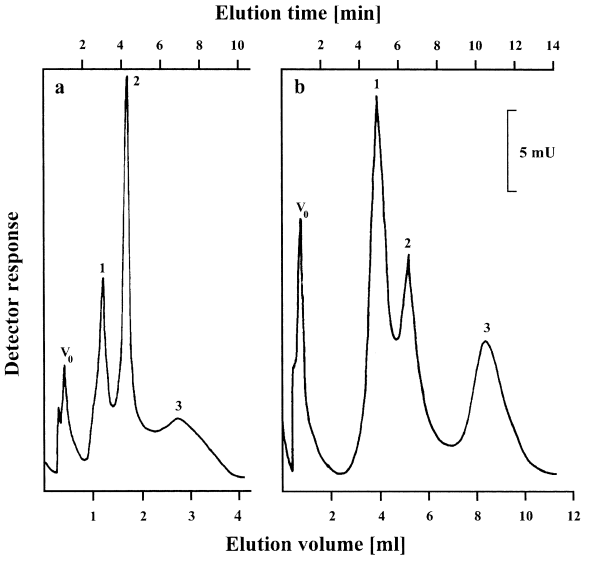


Fig. 6. Fractograms of the model silica mixture obtained in channel F at the flow-rate 0.4 ml/min (a) and in channel G at the flow-rate 0.8 ml/min (b). The symbols $V_0$, 1, 2, and 3 are used in the same way as in Fig. 2. The evaluation: (a) $R^*_{1,2}=2.7$, $R^*_{2,3}<1$, (b) unsuccessful.

nel G. Also the comparison of the sharpness of peaks 1 and 2 in Fig. 6a and Fig. 6b is in good agreement with the difference in the channel heights. The comparison of the separations obtained in channel G (Fig. 6b) and in the rectangular channel B (Fig. 2d) reveals that the effect of decreasing channel height did not provide any advantage.

## 4. Conclusions

Three channels of non-constant breadth and two channels of non-constant height have been tested and evaluated as tools for force field programming in GFFF. The optimizing potential of the effect caused by decreasing channel height and flow-velocity gradients achieved with the channels of non-constant cross-sections has been compared with the effects of the flow-rate gradients generated by a programmable pump using the same model mixture [28]. We aimed to improve the resolution of the first two peaks, to maintain the baseline resolution of the last two peaks of the sample and to increase the speed of separation. In general, the trapezoidal channels yielded reduced separation times. The best result was obtained with the gentle flow-velocity gradient generated by channel C at the flow-rate 0.5 ml/min. In this case, both resolution and speed of separation increased compared with the rectangular channel. At the flow-rate 0.2 ml/min, channel D yielded the shortest separation time without any loss of the resolution of the first two peaks compared with the rectangular channel. As the flow-velocity gradient enhanced and flow-rate increased, the height of peak 1 increased and the resolution of the first two peaks continuously deteriorated. The successful separations achieved with trapezoidal channels showed neither shorter separation times nor better resolution than those accomplished by a programmable pump [28]. Taking into account both resolution and speed of separation, we can conclude that the optimizing potential of trapezoidal channels is significantly lower than the potential of flow-rate gradients generated by a programmable pump. On the other hand, the problems with drifting baseline, which were shown in gradient separations achieved by the programmable pump, were not observed in the case of trapezoidal channels, and the instrumentation is much cheaper. Moreover, channels of other geometry (than trapezoidal one) can be easily tailored for specific separations.

The experiments carried out with channels of non-constant height did not yield advantageous separations. Moreover, the assembly of these channels is rather difficult in comparison to the channels of non-constant breadth.

## Acknowledgements

This work was supported by Grant no. A4031805/1998 from the Grant Agency of the Academy of Sciences of the Czech Republic.

## References

[1] J.C. Giddings, Sep. Sci. 1 (1966) 123.
[2] K.D. Caldwell, T.T. Nguyen, J.C. Giddings, M.N. Myers, Sep. Sci. Technol. 14 (1979) 935.
[3] J.C. Giddings, Sep. Sci. Technol. 18 (1983) 765.
[4] J. Janča, J. Chmelík, Anal. Chem. 56 (1984) 2481.
[5] J.C. Giddings, M.N. Myers, Sep. Sci. Technol. 13 (1978) 637.
[6] J.C. Giddings, M.N. Myers, K.D. Caldwell, J.W. Pav, J. Chromatogr. 185 (1979) 261.
[7] J. Pazourek, E. Urbánková, J. Chmelík, J. Chromatogr. A 660 (1994) 113.
[8] J. Pazourek, K.-G. Wahlund, J. Chmelík, J. Microcol. Sep. 8 (1996) 331.
[9] J. Pazourek, J. Chmelík, J. Microcol. Sep. 9 (1997) 611.
[10] R.E. Peterson II, M.N. Myers, J.C. Giddings, Sep. Sci. Technol. 19 (1984) 307.
[11] J. Pazourek, J. Chmelík, Chromatographia 35 (1993) 591.
[12] P.J.P. Cardot, J. Gerota, M. Martin, J. Chromatogr. 568 (1991) 93.
[13] A. Bernard, C. Bories, P.M. Loiseau, P.J.P. Cardot, J. Chromatogr. B 664 (1995) 444.
[14] E. Urbánková, A. Vacek, J. Chmelík, J. Chromatogr. B 687 (1996) 449.
[15] P.J.P. Cardot, J.M. Launay, M. Martin, J. Liq. Chromatogr. Relat. Technol. 20 (1997) 2543.
[16] J. Chmelík, A. Krumlová, J. Čáslavský, Chem. Pap. 52 (1998) 360.
[17] R. Sanz, L. Puignou, P. Reschiglian, M.T. Galceran, J. Chromatogr. A 919 (2001) 339.
[18] F.J.F. Yang, M.N. Myers, J.C. Giddings, Anal. Chem. 46 (1974) 1924.
[19] P.S. Williams, J.C. Giddings, Anal. Chem. 59 (1987) 2038.

[20] J.C. Giddings, V. Kumar, P.S. Williams, M.N. Myers, in: C.D. Craver, T. Provder (Eds.), Polymer Characterization: Physical Property, Spectroscopic, and Chromatographic Methods, ACS Advances in Chemistry Series 227. American Chemical Society, Washington, DC, 1990, Chapter 1.
[21] S.K. Ratanathanawongs, J.C. Giddings, Anal. Chem. 64 (1992) 6.
[22] J. Chmelík, J. Chromatogr. A 845 (1999) 285.
[23] P.S. Williams, T. Koch, J.C. Giddings, Chem. Eng. Commun. 111 (1992) 121.
[24] P.S. Williams, S.H. Lee, J.C. Giddings, Chem. Eng. Commun. 130 (1994) 143.
[25] V.L. Kononenko, J.K. Shimkus, J. Chromatogr. 520 (1990) 271.
[26] J. Plocková, J. Chmelík, J. Chromatogr. A 868 (2000) 217.
[27] J. Janoušková, M. Budinská, J. Plocková, J. Chmelík, J. Chromatogr. A 914 (2001) 183.
[28] J. Plocková, J. Chmelík, J. Chromatogr. A 918 (2001) 361.
[29] J. Chmelík, J. Janča, J. Liq. Chromatogr. 9 (1986) 55.
[30] J. Chmelík, M. Deml, J. Janča, Anal. Chem. 61 (1989) 912.
[31] J. Pazourek, J. Chmelík, J. Chromatogr. 593 (1992) 357.
[32] J. Pazourek, J. Liq. Chromatogr. 16 (1993) 69.
[33] A. Litzén, K.G. Wahlund, Anal. Chem. 63 (1991) 1001.
[34] K.G. Wahlund, J.C. Giddings, Anal. Chem. 59 (1987) 1332.